


Cite this: *RSC Adv.*, 2018, 8, 24866Received 28th March 2018  
Accepted 30th June 2018

DOI: 10.1039/c8ra02708k

rsc.li/rsc-advances

# Synthesis of core-shell N-TiO<sub>2</sub>@CuO<sub>x</sub> with enhanced visible light photocatalytic performance†

Shu Wang, Rufe Huo, Rui Zhang, Yuchuan Zheng, Changjiang Li and Le Pan \*

In this paper, a core-shell N-TiO<sub>2</sub>@CuO<sub>x</sub> nanomaterial with increased visible light photocatalytic activity was successfully synthesized using a simple method. By synthesizing ammonium titanyl oxalate as a precursor, N-doped TiO<sub>2</sub> can be prepared, then the core-shell structure of N-TiO<sub>2</sub>@CuO<sub>x</sub> with a catalyst loading of Cu on its surface was prepared using a precipitation method. It was characterized in detail using XRD, TEM, BET, XPS and H<sub>2</sub>-TPR, while its photocatalytic activity was evaluated using the probe reaction of the degradation of methyl orange. We found that the core-shell N-TiO<sub>2</sub>@CuO<sub>x</sub> nanomaterial can lessen the TiO<sub>2</sub> energy band-gap width due to the N-doping, as well as remarkably improving the photo-degradation activity due to a certain loading of Cu on the surfaces of N-TiO<sub>2</sub> supports. Therefore, a preparation method for a novel N, Cu co-doped TiO<sub>2</sub> photocatalyst with a core-shell structure and efficient photocatalytic performance has been provided.

## Introduction

Metallic oxides are important and widely used in catalysis, environmental science, ceramics, electronic devices and materials chemistry.<sup>1–4</sup> However, there are some disadvantages to single metallic oxides.<sup>5–7</sup> For example, anatase TiO<sub>2</sub> as a photocatalyst has many advantages, such as: cheapness, nontoxicity, stable chemical properties, degradation of organic matter and so on.<sup>8–13</sup> In the past twenty years, it has received wide attention. However, the band gap of 3.2 eV can only respond to UV light with a wavelength less than 387 nm.<sup>14–17</sup> The energy of ultraviolet light in sunlight only accounts for about 5%, so this seriously restricts the application of this photocatalyst to solar energy. If the scope of TiO<sub>2</sub> light absorption can be effectively expanded to visible light, its application will be greatly expanded, so this photocatalyst can make full use of solar energy, and the two major problems facing humanity, the energy crisis and environmental pollution, will be effectively solved.

Since Asahi<sup>18</sup> reported the semiconductor TiO<sub>2</sub> photocatalytic degradation of organic pollutants, crucial progress has been made by the doping of the element N, which causes the decrease of the band-gap of TiO<sub>2</sub> because of the element N. The amount of research on TiO<sub>2</sub> doped with N has been increasing.<sup>19–23</sup> In the process of the preparation of TiO<sub>2</sub>, a variety of physical and chemical methods are needed to prepare N-doped TiO<sub>2</sub>. These methods, without exception,

require nitrogen sources. On this basis, Fang<sup>24</sup> found that a N-doped TiO<sub>2</sub> photocatalyst could be obtained using ammonium titanyl oxalate as the precursor, and the efficiency of the process was greatly improved.

At the same time, the precious metals that have been reported with TiO<sub>2</sub> to improve the photocatalytic performance include precious metals such as Pt, Ag, Ir, Au, Ru, Pd, Rh and so on, among which there are the most reports about Pt, followed by Pd and Au.<sup>25–28</sup> The photocatalytic performance after Pt modification is the best, but comes with a higher cost. Ag modification leads to relatively less toxicity and has a lower cost. Therefore, the preparation of highly active noble metal doped photocatalysts by Ag deposition and modification is considered to be one of the important directions to improve photocatalytic activity in the future. Cu, Ag and Au elements belong to the same group of the periodic table IB, which means they may have a similar catalytic activity in the oxidation colour-fading reaction. However, the catalytic activity of CuO<sub>x</sub> was obviously lower than those of AgO<sub>x</sub> and AuO<sub>x</sub> due to the catalytic reaction on the surface of CuO<sub>x</sub> which has been shown to have a higher activation energy in previous research.<sup>29–31</sup>

In this paper, from the perspective of energy utilization and catalytic activity, we composed a new TiO<sub>2</sub> compound with N and Cu co-doped by a two-step method. When TiO<sub>2</sub> was synthesized, N doping was completed simultaneously using a suitable synthesis in the first step, which is different to the traditional method. There are many benefits to employing the new synthetic method of N-doped TiO<sub>2</sub>, such as: excellent reproducibility of sample synthesis, a better N-doped effect, and outstanding stability of catalytic activity based on “zero” loss of the N element. In the second step, the core-shell structure N-TiO<sub>2</sub>@CuO<sub>x</sub> catalyst was prepared by a precipitation method.

College of Chemistry and Chemical Engineering, Huangshan University, Huangshan 245041, China. E-mail: panle\_hs@163.com

† Electronic supplementary information (ESI) available. See DOI: 10.1039/c8ra02708k



The light energy which was absorbed by N doped  $\text{TiO}_2$  could be translated into the internal energy which was employed across the high energy barrier mentioned above. Then, their structures were examined with XRD, TEM, BET, and XPS. Lastly, we compared their catalytic activities using methyl orange degradation experiments. Therefore, an N, Cu co-doped  $\text{TiO}_2$  photocatalyst has been synthesized using a simple and low-cost process, and its core-shell structure and efficient photocatalytic performance have been studied.

## Results and discussion

Fig. S1† displays the concentration of methyl orange as a function of the reaction time over the different amounts of copper oxide in the catalytic system of  $\text{TiO}_2@0.1\text{CuO}_x$  and  $\text{N-TiO}_2@0.1\text{CuO}_x$  catalysts in UV, all wavelengths, and visible light respectively. This shows that the adsorption performance decreased and the catalytic activity increased as the  $\text{CuO}_x$  loading increased. Considering the above conditions, the total degradation performances of  $\text{TiO}_2@0.1\text{CuO}_x$  and  $\text{N-TiO}_2@0.1\text{CuO}_x$  showed maximum activities in the respective catalytic systems. Therefore, 0.1 $\text{CuO}_x$  was chosen in the later text and we do not specifically point out “0.1”.

Fig. 1 displays the XRD patterns of the  $\text{TiO}_2$  (A),  $\text{N-TiO}_2$  (B),  $\text{TiO}_2@0.1\text{CuO}_x$  (C) and  $\text{N-TiO}_2@0.1\text{CuO}_x$  (D) catalysts. The XRD patterns of the four catalysts all clearly show anatase  $\text{TiO}_2$  diffraction peaks, while only in the XRD pattern of  $\text{TiO}_2@0.1\text{CuO}_x$  (C) and  $\text{N-TiO}_2@0.1\text{CuO}_x$  (D) catalysts can we find  $\text{Cu}_2\text{O}$  diffraction peaks. These indicate the amount of  $\text{Cu}_2\text{O}$  nanoparticles formed when the copper nitrate was deposited on the surface of  $\text{TiO}_2$  and  $\text{N-TiO}_2$ .

Fig. 2 shows representative transmission electron microscopy (TEM) images of  $\text{TiO}_2$  (A),  $\text{N-TiO}_2$  (B),  $\text{TiO}_2@0.1\text{CuO}_x$  (C) and  $\text{N-TiO}_2@0.1\text{CuO}_x$  (D) catalysts. The TEM images of the four catalysts all clearly show the core and shell structures in the  $\text{TiO}_2@0.1\text{CuO}_x$  (C) and  $\text{N-TiO}_2@0.1\text{CuO}_x$  (D) catalysts, but not in the  $\text{TiO}_2$  (A) and  $\text{N-TiO}_2$  (B) catalysts.

Fig. 3 displays Ti 2p XPS patterns of the  $\text{TiO}_2$ ,  $\text{N-TiO}_2$ ,  $\text{TiO}_2@0.1\text{CuO}_x$  and  $\text{N-TiO}_2@0.1\text{CuO}_x$  catalysts. The Ti 2p XPS spectra of  $\text{TiO}_2$  and  $\text{N-TiO}_2$  can be nicely fitted with one component

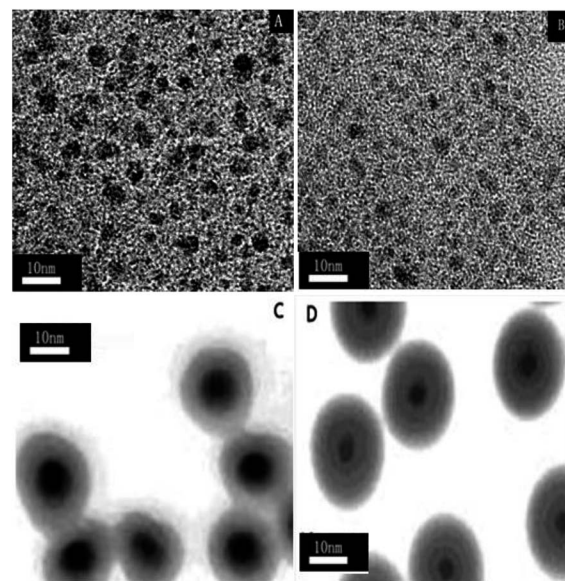


Fig. 2 Transmission electron microscopy (TEM) images of the  $\text{TiO}_2$  (A),  $\text{N-TiO}_2$  (B),  $\text{TiO}_2@0.1\text{CuO}_x$  (C) and  $\text{N-TiO}_2@0.1\text{CuO}_x$  (D) catalysts.

centring at 458.5 eV, which can be attributed to  $\text{Ti}^{4+}$  on the surface.<sup>32</sup> With the Cu loading on  $\text{TiO}_2$  and  $\text{N-TiO}_2$ , the Ti 2p peak shifts from 458.5 eV to 459.0 eV. Therefore, we hypothesize that the interaction between Ti and Cu on the interface contributes to this shift. While the Ti 2p XPS spectra of  $\text{TiO}_2@0.1\text{CuO}_x$  and  $\text{N-TiO}_2@0.1\text{CuO}_x$  fit with another component centring at 459.0 eV, the formation of the chemical bonds increases the binding energy of Ti,<sup>17</sup> which can be attributed to the complex species on the surfaces of core-shell structures.

Fig. 4 shows the Cu 2p<sub>3/2</sub> XPS patterns of the  $\text{TiO}_2@0.1\text{CuO}_x$  and  $\text{N-TiO}_2@0.1\text{CuO}_x$  catalysts. Table 1 shows the peak-fitting results of the Cu XPS spectra. We can observe that the  $\text{TiO}_2@0.1\text{CuO}_x$  and  $\text{N-TiO}_2@0.1\text{CuO}_x$  catalysts both show double peaks which are split in the Cu 2p<sub>3/2</sub> XPS patterns. As the binding energy is almost the same for  $\text{Cu}^0$  and  $\text{Cu}^+$  in XPS,<sup>33</sup> we cannot differentiate between the two peaks at low binding energies in the XPS spectra. As the 941–944 eV shake-up<sup>34</sup> is unique for  $\text{Cu}^{2+}$  in XPS spectra, and

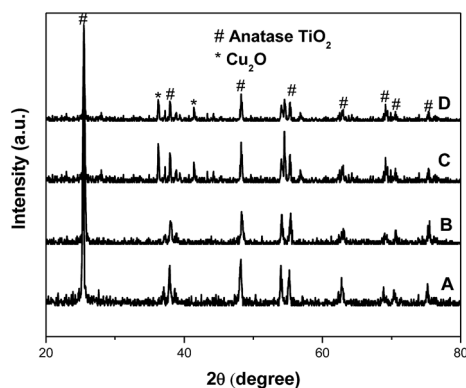


Fig. 1 XRD patterns of the  $\text{TiO}_2$  (A),  $\text{N-TiO}_2$  (B),  $\text{TiO}_2@0.1\text{CuO}_x$  (C) and  $\text{N-TiO}_2@0.1\text{CuO}_x$  (D) catalysts.

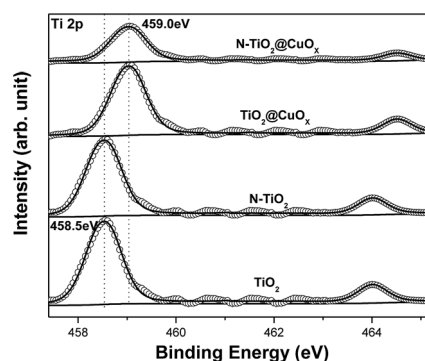


Fig. 3 Ti 2p XPS patterns of the  $\text{TiO}_2$ ,  $\text{N-TiO}_2$ ,  $\text{TiO}_2@0.1\text{CuO}_x$  and  $\text{N-TiO}_2@0.1\text{CuO}_x$  catalysts. Scattered circles and solid lines indicate the experimental data and fitting spectra, respectively.



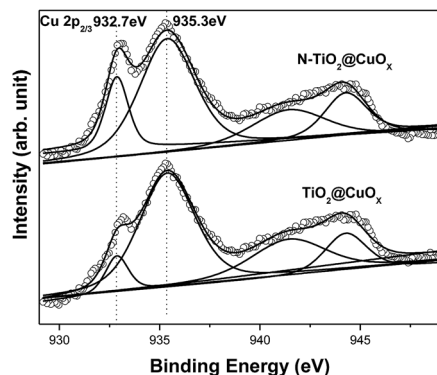


Fig. 4 Cu 2p<sub>3/2</sub> XPS patterns of the TiO<sub>2</sub>@CuO<sub>x</sub> and N-TiO<sub>2</sub>@CuO<sub>x</sub> catalysts. Scattered circles and solid lines indicate the experimental data and fitting spectra, respectively.

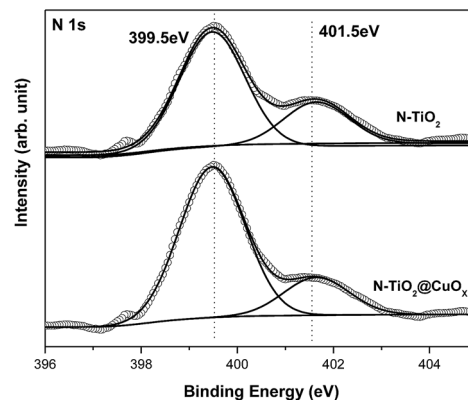


Fig. 5 N 1s XPS patterns of the N-TiO<sub>2</sub> and N-TiO<sub>2</sub>@CuO<sub>x</sub> catalysts. Scattered circles and solid lines indicate the experimental data and fitting spectra, respectively.

Table 1 Peak-fitting results of Cu XPS spectra of the TiO<sub>2</sub>@CuO<sub>x</sub> and N-TiO<sub>2</sub>@CuO<sub>x</sub> catalysts

Catalyst	Component 1		Component 2	
	BE (eV)	Fraction	BE (eV)	Fraction
TiO <sub>2</sub> @CuO <sub>x</sub>	932.7	9%	935.3	91%
N-TiO <sub>2</sub> @CuO <sub>x</sub>	932.7	25%	935.3	75%

the binding energy of Cu<sup>2+</sup> increases, we can confirm that it is the Cu<sup>2+</sup> that caused the peak at 935.3 eV. The difference between the Cu 2p<sub>3/2</sub> XPS spectra of the two samples is great, which indicates the different speciation which exists on their surfaces.

The following conclusions can be reached by analyzing the above results. When the copper nitrate was separately deposited on the surfaces of TiO<sub>2</sub> and N-TiO<sub>2</sub>, the content of Cu<sup>0</sup> and Cu<sup>+</sup> obtained on the surfaces of TiO<sub>2</sub> and N-TiO<sub>2</sub> was consistent with previous XRD results. Furthermore, we cannot find a peak due to CuO in the XRD patterns, but it is obvious in the XPS patterns. Therefore it can be hypothesized that the CuO on the surface of the catalysts was amorphous.

The N 1s XPS peak could be adequately fitted by two components with the N 1s binding energies at 399.5 and 401.5 eV in Fig. 5. We attribute the binding energy at 401.5 eV to the substitution with N in O-Ti-N,<sup>35</sup> while we attribute the binding energy at 399.5 eV to doped N in interstitial lattice sites, which can decrease the band gap from 3.2 eV to 2.4 eV.<sup>22</sup>

Fig. 6 and Table 2 show the N<sub>2</sub> adsorption-desorption isotherms and textural parameters of TiO<sub>2</sub>, N-TiO<sub>2</sub>, TiO<sub>2</sub>@CuO<sub>x</sub> and N-TiO<sub>2</sub>@CuO<sub>x</sub> respectively. The N<sub>2</sub> adsorption-desorption isotherms of TiO<sub>2</sub> and N-TiO<sub>2</sub>@CuO<sub>x</sub> are similar with H2 hysteresis loops according to IUPAC, which illustrate that the mesoporous structure exists on the surface of the catalysts.<sup>36</sup> We attribute the difference in absorption and desorption mechanisms to the “ink-bottle” pore.<sup>37</sup> The N<sub>2</sub> adsorption-desorption isotherms of N-TiO<sub>2</sub> show that the hysteresis loop is very wide with a high specific surface area and small size. The N<sub>2</sub> adsorption-desorption isotherm of TiO<sub>2</sub>@CuO<sub>x</sub> shows that the

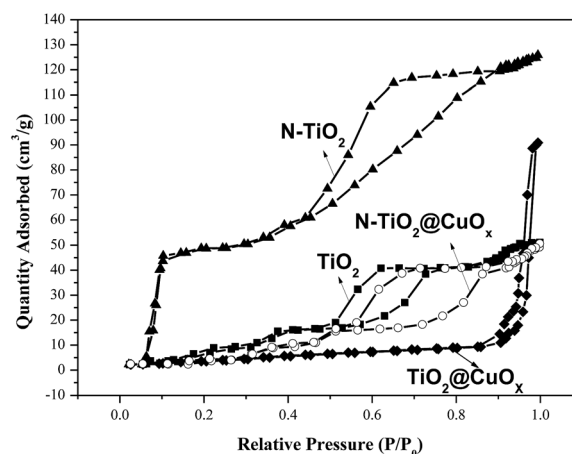


Fig. 6 The N<sub>2</sub> adsorption-desorption isotherms for TiO<sub>2</sub>, N-TiO<sub>2</sub>, TiO<sub>2</sub>@CuO<sub>x</sub> and N-TiO<sub>2</sub>@CuO<sub>x</sub>.

hysteresis loop shifts to the higher relative pressure ( $P/P_0 = 0.9$ ) between the H2 and H3 hysteresis loops according to the BDDT classification, which illustrates that the macro-pore structure exists on the surface of the support with a low specific surface area and big size.

Fig. S2† shows the concentration of methyl orange as a function of the reaction time over the TiO<sub>2</sub>, N-TiO<sub>2</sub>, TiO<sub>2</sub>@CuO<sub>x</sub> and N-TiO<sub>2</sub>@CuO<sub>x</sub> catalysts in UV light, all wavelengths and visible light. The degradation properties are composed of two parts, adsorption activity and photocatalytic activity, and

Table 2 Textural parameters of TiO<sub>2</sub>, N-TiO<sub>2</sub>, TiO<sub>2</sub>@CuO<sub>x</sub> and N-TiO<sub>2</sub>@CuO<sub>x</sub>

Support	Specific surface area (m <sup>2</sup> g <sup>-1</sup> )	Pore volume (cm <sup>3</sup> g <sup>-1</sup> )	Pore diameter (nm)
TiO <sub>2</sub>	38.2	0.195	22.4
N-TiO <sub>2</sub>	174	0.294	15.4
TiO <sub>2</sub> @CuO <sub>x</sub>	16.5	0.115	62.7
N-TiO <sub>2</sub> @CuO <sub>x</sub>	29.4	0.181	48.7



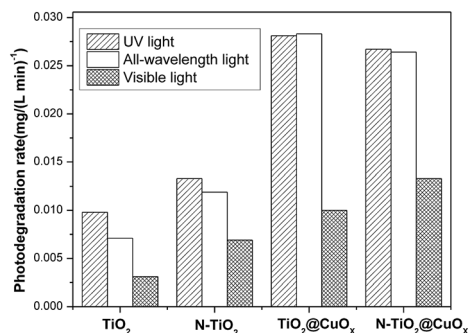


Fig. 7 Photo-degradation rate of the TiO<sub>2</sub>, N-TiO<sub>2</sub>, TiO<sub>2</sub>@CuO<sub>x</sub> and N-TiO<sub>2</sub>@CuO<sub>x</sub> catalysts in UV light, all wavelengths and visible light.

the degradation of methyl orange as the probe reaction was employed to respond to these two parts of the activity under different conditions. The results before the light illumination were characterized as adsorption activity, and after the light illumination as photocatalytic activity. Considering the results of BET and the adsorption and activity performance, we find that the adsorption performance is closely correlated to the specific surface area and size. Among the catalysts, N-TiO<sub>2</sub> has the best adsorption and TiO<sub>2</sub>@CuO<sub>x</sub> has the worst, while N-TiO<sub>2</sub>@CuO<sub>x</sub> is close to TiO<sub>2</sub> which is in the middle. We can conclude from the results of XPS, TEM and the absorption data that N-doping can effectively improve the absorption by the catalyst, but the core-shell structure may have an adverse effect.

Fig. 7 and 8 display the photo-degradation rate and total degradation rate of the TiO<sub>2</sub>, N-TiO<sub>2</sub>, TiO<sub>2</sub>@CuO<sub>x</sub> and N-TiO<sub>2</sub>@CuO<sub>x</sub> catalysts in UV light, all wavelengths and visible light. The catalytic activity of N-TiO<sub>2</sub> is much better than that of TiO<sub>2</sub> in visible light, and also of N-TiO<sub>2</sub>@CuO<sub>x</sub> and TiO<sub>2</sub>@CuO<sub>x</sub>. We can make a conclusion that N-doping can effectively reduce the band gap of energy of TiO<sub>2</sub> and improve the use of visible light.

Fig. 9 shows the UV-vis diffuse reflection spectra of N-TiO<sub>2</sub> and N-TiO<sub>2</sub>@CuO<sub>x</sub>. The N-TiO<sub>2</sub> and N-TiO<sub>2</sub>@CuO<sub>x</sub> catalysts exhibit a pale yellow colour. The UV-vis diffuse reflection spectra of these two catalysts show a continuous and tailing

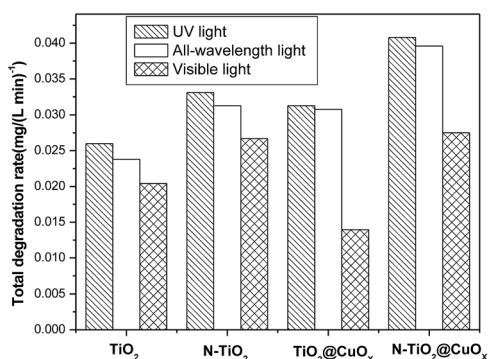


Fig. 8 Total degradation rate of TiO<sub>2</sub>, N-TiO<sub>2</sub>, TiO<sub>2</sub>@CuO<sub>x</sub> and N-TiO<sub>2</sub>@CuO<sub>x</sub> catalysts in UV light, all wavelengths and visible light respectively.

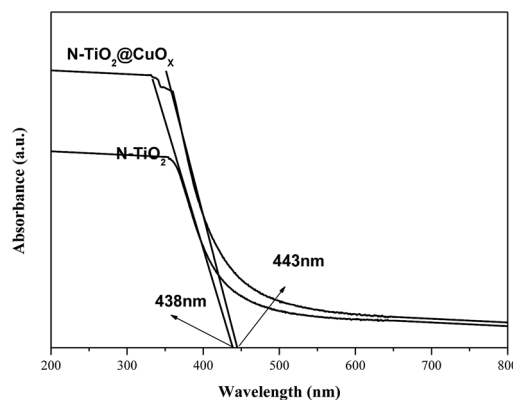


Fig. 9 UV-vis diffuse reflection spectra for the catalysts N-TiO<sub>2</sub> and N-TiO<sub>2</sub>@CuO<sub>x</sub>.

absorption in the visible region. The band-gap energies of the N-TiO<sub>2</sub> and N-TiO<sub>2</sub>@CuO<sub>x</sub> catalysts are 2.83 and 2.80 eV, respectively, which were determined by the plot of the modified Kubelka-Munk function  $(\alpha h\nu)^{1/2}$  versus photon energy assuming indirect transitions.<sup>38</sup> Based on the above data, we can make a conclusion that N-doping can effectively reduce the band gap of energy of TiO<sub>2</sub> in N-TiO<sub>2</sub> and N-TiO<sub>2</sub>@CuO<sub>x</sub> catalysts.

Fig. 10 shows the H<sub>2</sub>-TPR spectra of the catalysts of TiO<sub>2</sub>@CuO<sub>x</sub> and N-TiO<sub>2</sub>@CuO<sub>x</sub>. The H<sub>2</sub>-TPR of CuO supported on CeO<sub>2</sub> has been extensively investigated.<sup>39–42</sup> CuO is reduced below 300 °C and the reduction temperature of different CuO species on CeO<sub>2</sub> follows the order: finely dispersed CuO < large CuO crystallites < bulk CuO. Therefore, the reduction peak at 221 °C is assigned to the reduction of finely dispersed CuO, and that at 258 °C to the reduction of large CuO crystallites and bulk CuO.<sup>43</sup>

Considering the results from H<sub>2</sub>-TPR and the photo-degradation performance of TiO<sub>2</sub>@CuO<sub>x</sub> and N-TiO<sub>2</sub>@CuO<sub>x</sub> catalysts in UV and all-wavelength light, the activity increases as the size of CuO decreases on the surface. However, the reason for the activity of TiO<sub>2</sub>@CuO<sub>x</sub> being worse than N-TiO<sub>2</sub>@CuO<sub>x</sub> in visible light can be attributed to the decrease in efficiency for visible light.

On the basis of TEM, BET, H<sub>2</sub>-TPR, XPS, the catalytic activity performance and the stability results, the interfacial structures

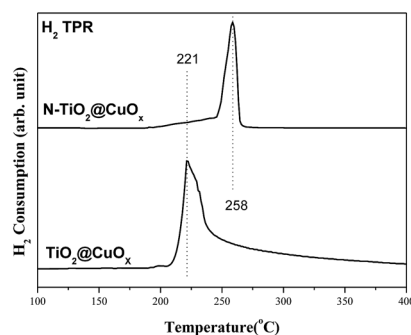


Fig. 10 H<sub>2</sub>-TPR spectra of the catalysts TiO<sub>2</sub>@CuO<sub>x</sub> and N-TiO<sub>2</sub>@CuO<sub>x</sub>.





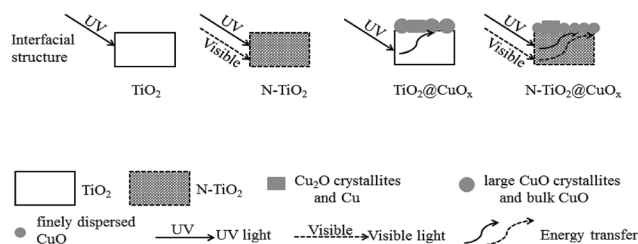


Fig. 11 Schematic illustration of the interfacial structures of  $\text{TiO}_2$ ,  $\text{N-TiO}_2$ ,  $\text{TiO}_2@\text{CuO}_x$  and  $\text{N-TiO}_2@\text{CuO}_x$  and their responses to different wavelengths of light.

of  $\text{TiO}_2$ ,  $\text{N-TiO}_2$ ,  $\text{TiO}_2@\text{CuO}_x$  and  $\text{N-TiO}_2@\text{CuO}_x$  and their responses to different wavelengths of light are schematically illustrated in Fig. 11. These results demonstrate that the

interfacial reaction mechanisms on the surfaces of  $\text{TiO}_2@\text{CuO}_x$  and  $\text{N-TiO}_2@\text{CuO}_x$  are the same. The light energy which was absorbed by  $\text{TiO}_2$  and  $\text{N-doped TiO}_2$  is translated into the internal energy which was employed to overcome the energy barrier of the reaction on the  $\text{CuO}_x$  surface. The difference is simply the wavelengths of light which are responded to by  $\text{TiO}_2$  and  $\text{N-doped TiO}_2$ .

Fig. 12 shows the stability of  $\text{N-TiO}_2@\text{CuO}_x$  in UV light, all wavelengths, and visible light, and obviously shows that there is hardly any absorption performance, although the activity performances are almost unchanged during the 40 hours. We consider that the  $\text{N-TiO}_2@\text{CuO}_x$  catalyst is a kind of reusable material to degrade the methyl orange.

## Experimental

### Catalyst preparation

We prepared two solutions by adding 20.0 g oxalic acid to 200 mL distilled water for both, then dripped 10 mL titanium tetrachloride into both of them dropwise, and stirred them evenly. After the drops were added, we added sodium hydroxide and ammonia solution respectively to adjust the pH values of the solutions to 8–9. We continuously stirred the above solutions for 8 h, after which white precipitates were produced. After the agitation, we aged them for 8 h, and then filtered out these white precipitates. These white precipitates were washed with distilled water and ethanol several times until there was no chloride in the filtrate, then dried at 70 °C and calcined for 2 h at 400 °C in sequence. These two obtained products were recorded as  $\text{TiO}_2$  and  $\text{N-TiO}_2$ , respectively.

The above  $\text{TiO}_2$  (5 g) and  $\text{N-TiO}_2$  (5 g) were ground to powders and each was put into a three-neck bottle. Then we added 5 mL copper nitrate solution ( $1.06 \text{ mol L}^{-1}$ ) and distilled water to both of them and stirred them at 70 °C for 30 min. Then we added sodium hydroxide and ammonia solution respectively to adjust the pH values of the solutions to 8–9 separately, and stirred them at 70 °C for 24 h. Then we filtered these solids, washed them with distilled water and ethanol several times, dried them at 70 °C for 12 h, and calcined them in air at 400 °C for 4 h. These two obtained products were recorded as  $\text{TiO}_2@\text{CuO}_x$  and  $\text{N-TiO}_2@\text{CuO}_x$  respectively.

### Catalyst characterization

Powder X-ray diffraction (XRD) patterns were acquired on a Philips X'Pert PRO SUPER X-ray diffractometer with a Ni-filtered  $\text{Cu K}\alpha$  X-ray source operating at 40 kV and 50 mA. X-ray photoelectron spectroscopy (XPS) measurements were performed on an ESCALAB 250 electron spectrometer using a monochromatized  $\text{Al K}\alpha$  excitation source ( $h\nu = 1486.6 \text{ eV}$ ). Transmission electron microscopy (TEM) measurements were carried out on a JEOL-2100F transmission electron microscope at an accelerating voltage of 200 kV.  $\text{N}_2$  adsorption-desorption isotherms (BET) were acquired on a Beckman Coulter SA3100 surface area analyzer, in which the sample was degassed at 300 °C for 30 min under a nitrogen atmosphere prior to the measurements. The reduction behaviors of the catalysts were

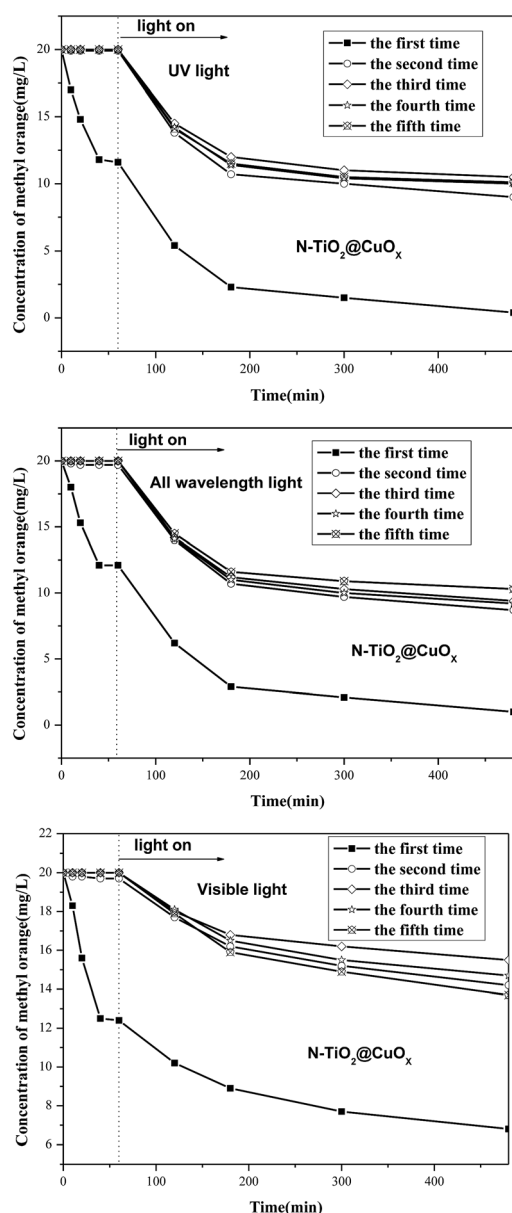


Fig. 12 Stability of the  $\text{N-TiO}_2@0.1\text{CuO}_x$  in UV light, all wavelengths, and visible light.



measured using H<sub>2</sub> temperature-programmed reduction (H<sub>2</sub>-TPR) techniques. UV-vis absorption spectra were recorded using a SolidSpec-DUV-3700 DUV-vis-NIR spectrometer.

### Degradation property measurements

The degradation property is composed of two parts, the adsorption activity and the photocatalytic activity. We employed the degradation of methyl orange as the probe reaction. We added 0.12 g catalyst to 20 mg L<sup>-1</sup> methyl orange aqueous solution (40 mL), and stirred it for 1 h whilst avoiding light. We subjected the catalyst to the different wavelengths of irradiation, and took the supernatant to measure the concentration of methyl orange at different time points. The results before the light illumination were characterized as adsorption activity, and after the light illumination as photocatalytic activity.

## Conclusions

A novel N, Cu co-doped TiO<sub>2</sub> photocatalyst with a core-shell structure has been prepared using a simple method and the structure-adsorption-photo-degradation activity relationships of TiO<sub>2</sub> base catalysts were examined using the probe reaction of the degradation of methyl orange. The results suggested that the N-TiO<sub>2</sub>@CuO<sub>x</sub> nanomaterial can reduce the band gap width of TiO<sub>2</sub> by N-doping. Meanwhile, we found the photo-degradation rate of catalysts clearly improved with a certain loading of Cu on the surfaces of N-TiO<sub>2</sub>. Consequently, we synthesized an efficient N-doped TiO<sub>2</sub>@CuO<sub>x</sub> photocatalyst with a core-shell structure.

## Conflicts of interest

There are no conflicts to declare.

## Acknowledgements

This work was supported by the National Natural Science Foundation of China (21401065), the Undergraduate Training Programs for Innovation, Entrepreneurship of China (201710375026, 201710375012) and the Natural Science Foundation of Huangshan University (2011xkj014, 2015xkj003).

## Notes and references

- Q. Hua, T. Cao, X. K. Gu, J. Q. Lu, Z. Q. Jiang, X. R. Pan, L. F. Luo, W. X. Li and W. X. Huang, *Angew. Chem., Int. Ed.*, 2014, **53**, 4856–4861.
- Q. Hua, T. Cao, H. Z. Bao, Z. Q. Jiang and W. X. Huang, *ChemSusChem*, 2013, **6**, 1966–1972.
- H. B. Tao, L. W. Fan, J. Z. Chen, H. B. Yang, J. J. Gao, J. W. Miao, S. L. Chen and B. Liu, *J. Am. Chem. Soc.*, 2016, **138**, 9978–9985.
- C. Y. Hou, M. W. Zhang, T. S. Kasama, C. Engelbrekt, L. L. Zhang, H. Z. Wang and Q. J. Chi, *Adv. Mater.*, 2016, **28**, 4097–4104.
- N. Serpone, I. Texier, A. V. Emerline, P. Pichat, H. Hidaka and J. Zhao, *J. Photochem. Photobiol., A*, 2000, **136**, 145–246.
- M. M. Aboelnga and J. W. Gauld, *J. Phys. Chem. B*, 2017, **121**, 6163–6174.
- A. Dawson and V. K. Prashant, *J. Phys. Chem. B*, 2001, **105**, 960–966.
- W. Z. Fang, M. Y. Xing and J. L. Zhang, *J. Photochem. Photobiol., C*, 2017, **32**, 21–39.
- F. Jiang, Z. Zheng, Z. Y. Xu, S. R. Zheng, Z. B. Guo and L. Q. Chen, *J. Hazard. Mater.*, 2006, **134**, 94–103.
- G. Colon, M. C. Hidalgo and J. A. Navio, *Appl. Catal., B*, 2003, **45**, 39–50.
- P. Mohapatra, S. K. Samantaray and K. Parida, *J. Photochem. Photobiol., A*, 2005, **170**, 189–194.
- A. Nakajima, H. Obata, Y. Kameshima and K. Okada, *Catal. Commun.*, 2005, **6**, 716–720.
- X. C. Wang, J. C. Yu, P. Liu, X. X. Wang, W. Y. Su and X. Z. Fu, *J. Photochem. Photobiol., A*, 2006, **179**, 339–347.
- F. Nemati and A. Elhampour, *Res. Chem. Intermed.*, 2016, **42**, 7611–7624.
- J. Fang, F. C. Shi, J. J. Ding, S. T. Xu, J. Bao, Y. S. Ma, J. Q. Jiang, W. P. Zhang and W. X. Huang, *J. Phys. Chem. C*, 2010, **114**, 7940–7948.
- J. Fang, H. Z. Bao, B. He, F. Wang, D. J. Si, Z. Q. Jiang, Z. Y. Pan, S. Q. Wei and W. X. Huang, *J. Phys. Chem. C*, 2007, **111**, 19078–19085.
- J. Fang, X. Z. Bi, D. J. Si, Z. Q. Jiang and W. X. Huang, *Appl. Surf. Sci.*, 2007, **253**, 8952–8961.
- R. Asahi, T. Morikawa, T. Ohwaki, K. Aoki and Y. Taga, *Science*, 2001, **293**, 269–271.
- X. W. Cheng, H. L. Liu, Q. H. Chen, J. J. Li and P. Wang, *Electrochim. Acta*, 2013, **103**, 134–142.
- H. Irie, Y. Watanabe and K. Hashimoto, *J. Phys. Chem. B*, 2003, **107**, 5483–5486.
- O. Diwald, T. L. Thompson and T. Zubkov, *J. Phys. Chem. B*, 2004, **108**, 6004–6008.
- O. Diwald, T. L. Thompson and E. G. Goralski, *J. Phys. Chem. B*, 2004, **108**, 52–57.
- S. Yin, H. Yamaki and M. Komatsu, *J. Mater. Chem.*, 2003, **13**, 2996–3001.
- J. Fang, F. Wang, K. Qian, H. Z. Bao, H. X. Sun, Z. Q. Jiang and W. X. Huang, *J. Phys. Chem. C*, 2008, **112**, 18150–18156.
- D. M. Blake, *NREL/TP-430-6084*, National Renewable Energy Laboratory, Golden, Co, 1994.
- D. M. Blake, *NREL/TP-340-22197*, National Renewable Energy Laboratory, Golden, Co, 1997.
- D. M. Blake, *NREL/TP-570-26797*, National Renewable Energy Laboratory, Golden, Co, 1999.
- D. M. Blake, *NREL/TP-640-28297*, National Renewable Energy Laboratory, Golden, Co, 2002.
- B. White, M. Yin, A. Hall, D. Le, S. Stolbov, T. Rahman, N. Turro and S. O'Brien, *Nano Lett.*, 2006, **6**, 2095–2098.
- M. F. Luo, J. M. Ma, J. Q. Lu, Y. P. Song and Y. J. Wang, *J. Catal.*, 2007, **246**, 52–59.
- G. Avgouropoulos and T. Ioannides, *Appl. Catal., B*, 2006, **67**, 1–11.
- J. F. Moulder, W. F. Stickle, P. E. Sobol and K. D. Bomben, *Handbook of X-ray Photoelectron Spectroscopy*, Perkin-Elmer Corporation, Eden Prairie, MN, 1992.



- 33 G. Schon, *Surf. Sci.*, 1973, **35**, 96–108.
- 34 C. C. Chusuei, M. A. Brookshier and D. W. Goodman, *Langmuir*, 1999, **15**, 2806–2808.
- 35 X. Chen and C. Burda, *J. Phys. Chem. B*, 2004, **108**, 15446–15449.
- 36 X. Yang, Y. H. Wang, L. L. Xu, X. D. Yu and Y. H. Guo, *J. Phys. Chem. C*, 2008, **112**, 11481–11489.
- 37 H. G. Yu, S. C. Lee, J. G. Yu and C. H. Ao, *J. Mol. Catal. A: Chem.*, 2006, **246**, 206–211.
- 38 I. Motoki, Y. Keiji, K. Tsutomu, O. P. M. Orlando, O. Bunsho and W. Hisanobu, *Appl. Catal., B*, 2013, **132–133**, 39–44.
- 39 M. F. Luo, J. M. Ma, J. Q. Lu, Y. P. Song and Y. J. Wang, *J. Catal.*, 2007, **246**, 52–59.
- 40 H. B. Zou, X. F. Dong and W. M. Lin, *Appl. Surf. Sci.*, 2006, **253**, 2893–2898.
- 41 T. Caputo, L. Lisi, R. Pirone and G. Russo, *Appl. Catal., A*, 2008, **348**, 42–53.
- 42 X. L. Tang, B. C. Zhang, Y. Li, Y. D. Xu, Q. Xin and W. J. Shen, *Appl. Catal., A*, 2005, **288**, 116–125.
- 43 K. Qian, Z. X. Qian, Q. Hua, Z. Q. Jiang and W. X. Huang, *Appl. Surf. Sci.*, 2013, **273**, 357–363.

